Bidisperse Mixed Brushes: Synthesis and Study of Segregation in Selective Solvent

Sergiy Minko,*,†,‖ Igor Luzinov,‡ Valeriy Luchnikov,† Marcus Müller,§ Satish Patil,† and Manfred Stamm†

Institut für Polymerforschung Dresden, Hohe Strasse 6, D-01069 Dresden, Germany; School of Materials Science and Engineering, Clemson University, Clemson, South Carolina 29634; and Institut für Physik, WA331, J. Gutenberg Universität, D-55099 Mainz, Germany

Received February 6, 2003; Revised Manuscript Received April 17, 2003

ABSTRACT: We prepare a series of mixed brushes of two incompatible polymers, polystyrene (PS) and poly(2-vinylpyridine) (P2VP) grafted by end groups to Si wafers from carboxyl-terminated P2VP (M_W-(P2VP) 42 kg/mol) and carboxyl-terminated PS. The molecular mass of PS ranged from 2.98 to 75 kg/mol. The mixed brushes are bidisperse (asymmetric) with respect to the difference of molecular mass of P2VP and PS while the polydispersity of PS and P2VP is narrow. We expose the mixed brushes to selective solvents (toluene for PS and ethanol for P2VP). The morphology and surface chemical composition are investigated using scanning probe microscopy and contact angle measurements. For small chain length asymmetry, the brushes exhibit lateral and perpendicular segregation, and the structure depends on the solvent quality. Upon increasing the molecular weight asymmetry, we encounter the transition from a morphology of laterally segregated domains to a layered (sandwich-like) structure. The location of this transition can be tuned by changing the solvent selectivity. We find qualitative agreement between experiments and self-consistent-field calculations.

Introduction

Polymer brushes find practical applications for colloidal stabilization and controlling surface properties (thin film stability/dewetting, adhesion, patterned surfaces, protein adsorption, etc.).[1,2] For this reason polymer brushes have also attracted much theoretical interest. The study of polymer brushes started with the pioneering works of Alexander,[3] de Gennes,[4] Cantor,[5] Semenov,[6] Milner et al.,[7] and Zhulina et al.[8] These approaches calculated the brush profile and explored analytically the dependencies on molecular weight and grafting density. The main theoretical predictions were supported experimentally.[9−12] More recently, brushes in a bad solvent and mixed brushes have been studied. If the chain ends are immobile on the grafting surface, these systems will exhibit also lateral structure and thereby allow for the study of self-assembly and offer opportunities to fabricate functional materials. In the present study we explore the behavior of a polymer brush which consists of two incompatible polymers of different lengths with immobile grafting points.

The behavior of binary brushes composed of two compatible polymers which differ in their molecular weights has been studied theoretically[13−20]and experimentally.[21−29] Both approaches find a stratification of the bidisperse brush: the bottom of the brush is composed of short and long chains forming a mixed region, while the top of the brush is occupied predominantly by long chains. There is no sharp segregation between those regions but a rather gradual variation of the fraction of long chains as a function of the distance from the surface.

* Corresponding author: telephone: 315-268-3807, fax: 315-268-6610, e-mail: sminko@clarkson.edu.
† Institut für Polymerforschung Dresden.
‡ Clemson University.
§ J. Gutenberg Universität.
‖ Present address: Department of Chemistry, Clarkson University, Potsdam, New York 13699-5810.

Mixed brushes prepared from polymers of similar molecular weight but different chemical compositions have also been analyzed theoretically[30−32] and investigated experimentally.[32−34] The brush can exhibit lateral and perpendicular (sandwich-like) segregation which can be controlled by composition, incompatibility, and solvent quality. Lateral structure formation is dominant in nonselective solvents and results in a ripple morphology; i.e., the two components segregate into elongated domains or stripes. The lateral length scale is on the order of the molecules' extension (Scheme 1a). If the solvent is bad for one component, this polymer will form clusters embedded in a matrix (dimple morphology) of the other polymer. The matrix component is enriched at the brush's top, while the component that forms the dimples prevails at the bottom of the brush (Scheme 1b). This self-assembly determines the surface energetic state and functionality. It can be controlled by exposing the brush to different environments.

In this paper, we combine both types of asymmetry; i.e., we systematically study mixed brushes prepared from two polymers of different chemical compositions and molecular weights irreversibly grafted onto Si wafers. Neither theoretical nor experimental investigations were performed for brushes that combine these types of asymmetry. This asymmetry is of practical importance: first, any synthetic route of fabrication can introduce these types of asymmetry in an experiment. Second, controlled asymmetry in molecular weights might help to regulate the morphology of the mixed brush. Intuitively, the difference in molecular weights of both components will amplify perpendicular segregation if the solvent is nonselective or good for the longer chains. If the solvent is worse for the longer chains than for the shorter ones, solvent quality and chain length asymmetry counteract. In this paper we study the response of the mixed brush to molecular weight asymmetry and solvent selectivity by experiments and self-consistent-field calculations.

10.1021/ma034160h CCC: $25.00
Published on Web 08/26/2003

Scheme 1. Schematic Illustration of Two Possible Morphologies of Mixed Brush Irreversibly Grafted to Solid Substrates (Cross Section of the Layer): Ripple Morphology in a Nonselective Solvent (a); Dimple Morphology in a Solvent Poor for the Black Chains (b)

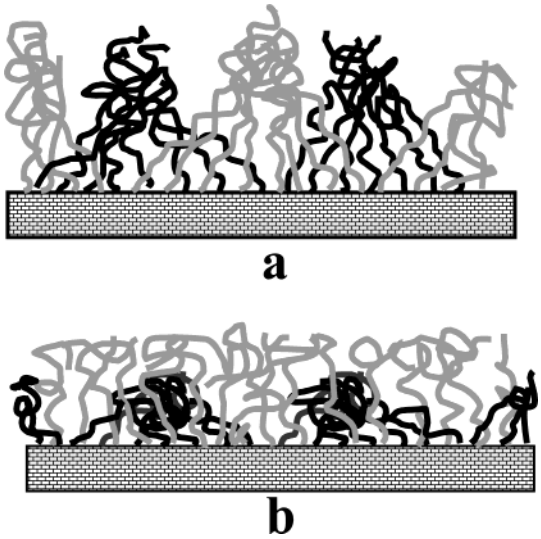

Experimental Section

Materials. Carboxyl-terminated polystyrene PS16K (M_n = 16 900 g/mol, M_w = 21 900 g/mol) synthesized by atom free living polymerization using 4-(1-bromoethyl)benzoic acid as initiator was kindly offered by Dr. J. Pionteck. Carboxyl-terminated PS of other molecular weights PS2K (M_n = 2000 g/mol, M_w = 2980 g/mol), PS9K (M_n = 9700 g/mol, M_w = 10 600 g/mol), PS45K (M_n = 45 900 g/mol, M_w = 48 400 g/mol), PS72K (M_n = 72 300 g/mol, M_w = 75 200 g/mol), and poly(2-vinylpyridine) (P2VP42K; M_n = 39 200 g/mol and M_w = 41 500 g/mol) were purchased from Polymer Source, Inc. (synthesized by anionic polymerization). Toluene and tetrahydrofuran (THF) were distilled after drying over sodium. Highly polished silicon wafers (obtained from Wacker-Chemitronics) were first cleaned in an ultrasonic bath for 30 min with dichloromethane, placed in cleaning solution (prepared from NH_4OH and H_2O_2) at 60 °C for 1 h, and then rinsed several times with Millipore water (18 MΩ cm^{-1}). 3-Glycidoxypropyltrimethoxysilane (GPS) ABCR (Karlsruhe, Germany) was used as received.

Preparation of the Binary Brushes. We employ a recently reported method[34,35] for grafting an end-terminated polymer from the melt. GPS was chemisorbed on the surface of cleaned Si wafers from 1% solution in the dried toluene for 16 h at room temperature. Afterward, the samples were carefully rinsed with toluene and ethanol to remove nongrafted GPS. In the next step a thin film (50 ± 5 nm as measured with ellipsometry) of PS was spin-coated on the top of the GPS layer from the 1% toluene solution. Then the film was heated to 150 °C in a vacuum oven for different periods of time to graft PS and to study the kinetics of grafting.[34] The nongrafted polymer was removed by Soxhlet extraction with toluene for 5−7 h. The conditions of the PS grafting were chosen such that in this step we grafted only half of the maximal amount that would be achieved in the long time limit. Then the second polymer P2VP was spin-coated on top of the film, and the heating procedure followed by subsequent Soxhlet extraction to remove any nongrafted polymer was performed. The inverse sequence of grafting (first P2VP and then PS) was not successful; the grafting was not homogeneous. This indicates the importance of the affinity of P2VP to the SiO_2 surface which acts as a driving force for P2VP to penetrate PS brush and to attach to the functional groups of the grafting surface. The properties of the brush were studied with FTIR-ATR, XPS, ellipsometry, and X-ray reflectivity experiments. Details were reported elsewhere.[34]

Sample Characterization. *Ellipsometry*. Layer thickness and grafted amounts were evaluated at λ = 633 nm and an angle of incidence of 70° using a Multiscope Optrel (Berlin, Germany) null ellipsometer with XY-positioning table for mapping of the sample surface. The lateral resolution is set by the beam spot of about 2 mm. Measurements were performed for each sample after each step of the synthesis. Measurements of the previous step were used as a reference for the simulation of ellipsometry data. Initially, the thickness of native SiO_2 layer (usually 1.4 ± 0.2 nm) was calculated using refractive indexes N_d = 3.858-i0.018 for the Si substrate and n = 1.4598 for the SiO_2 layer. The thickness of the GPS layer (typically 1.4 ± 0.3 nm) was evaluated using a two-layer model SiO_2/GPS using a refractive index of GPS equal to 1.429. The thickness of PS or P2VP as the first grafted layer (typically 1−7 nm) was evaluated with a three-layer model SiO_2/GPS/PS using n = 1.59 or, in the case of SiO_2/GPS/P2VP, n = 1.595. Finally, the thickness of the whole polymer film (typically 5−8 nm) after grafting of the second polymer was calculated using a three-layer model SiO_2/GPS/polymer where we regard the thin polymer film as an effective optical medium with n = 1.59. From these values we calculated the grafted amount of each polymer $A = H\rho$ and grafting density $\Sigma = AN_{Av}/M_w$, where H is the ellipsometric thickness, ρ the bulk polymer density, N_{Av} Avogadro's number, and M_w the molecular weight. The morphology of the film and its roughness change upon exposure to different solvents. Nevertheless, this does not affect ellipsometry data because of the small difference between refractive indexes of PS and P2VP and the small absolute value of root-mean-square roughness (rms) of the films. The roughness (rms) ranges from 0.3 to 1 nm, and this value is on the order of a polymer segment. The results of ellipsometry measurements agree very well with the thickness of each layer evaluated from the simulation of X-ray reflectivity data.[34]

Scanning probe microscopy (SPM) studies were performed on a Dimension 3100 (Digital Instruments, Inc.) microscope. We used tapping and phase modes to study the surface morphology of the films in ambient air. Silicon tips with spring constants of 50 N/m were used. Imaging was done at scan rates in the range 1−2 Hz. The free amplitude for scanning probe, A_0, was chosen about 40 nm. For "light" and "moderate" tapping modes, the set-point amplitude ratio, $r_{sp} = A_{sp}/A_0$ (A_{sp} is the set-point amplitude used for the feedback control), was selected to 0.9 ± 0.05 and 0.65 ± 0.05, respectively.[36−38] Power spectra density plots (PDS) representing Fourier transform of the topography SPM images were evaluated using commercial software. A maximum in a PDS plot is associated with a dominant lateral length scale of the segregated polymer brush.

The advancing *contact angle* of water was measured using DSA Krüss (Hamburg, Germany) equipment. To estimate the fraction of each polymer on the surface, we used the Cassie equation $\cos\theta_{1,2} = f_1\cos\theta_1 + f_2\cos\theta_2$, where f_1 and f_2 represent the phase fractions, θ_1 and θ_2 are the measured contact angles for the pure polymers (90° for PS and 60° for P2VP), and $\theta_{1,2}$ is the contact angle for the brush. The brushes exhibit a rms ranging from 0.3 to 1 nm. Using homopolymer brushes for reference experiments, we found that this range of roughness caused no effect on contact angle values.

Study of Switching Behavior. The samples of Si wafers with the grafted PS/P2VP mixed brushes were exposed for 10 min to solvents of different quality for the components. After each treatment with a particular solvent the samples were dried in a flow of nitrogen. We rapidly measured the contact angle and studied the sample by AFM. The experiments were repeated several times with each sample to verify the reversibility of the switching of surface properties. In these experiments we assume that the morphology of the dry film is directly correlated with the structure of the swollen film. Time of switching in a particular solvent is on the order of minutes (contact angle changes in 1−2 min and approaches to equilibrium in 5−10 min). It is much larger than time to dry the film under nitrogen flux (several seconds). Therefore, we assume that we freeze the film morphology during solvent evaporation. At ambient conditions the dry polymer film is in

glassy state, and the film morphology is stable for a long period of time.

Results and Discussion

SCF Calculations. We consider a binary brush that contains the same number of polymers of each type, *A* and *B*. Polymers of both types are modeled by Gaussian chains with equal statistical segment length. *Z* denotes the distance from the grafting plane. The mean end-to-end distance of the free (nongrafted) chain in θ-conditions $h_\theta{}^A$ is taken to be the unit of length. Each *A* chain comprises *N* segments, and each *B* chain contains αN segments, where α denotes the chain length asymmetry. We describe the structure of the brush by the segment number densities, $\rho^A(\vec{r})$ and $\rho^B(\vec{r})$, which we compute in the framework of the self-consistent-field theory (SCF). The SCF free energy functional has the form

$$\beta F = \beta U(\rho^A,\rho^B) - \int w^A\rho^A \,\mathrm{d}\vec{r} - \int w^B\rho^B \,\mathrm{d}\vec{r} - \sum_{r_0} \ln Q_{r_0}{}^A - \sum_{r_0} \ln Q_{r_0}{}^B \quad (1)$$

where $\beta = 1/kT$ denotes the inverse temperature, $Q_{r_0}{}^A$, $Q_{r_0}{}^B$ are the partition functions of single *A* and *B* chains in the effective fields w^A, w^B, and each chain is identified by its immobile grafting point, r_0. As interaction free energy functional we employ a third-order virial expansion

$$U(\rho^A,\rho^B) = \nu\int\left\{\frac{1}{2}(\rho^A+\rho^B)^2 - \frac{\chi}{4}(\rho^A-\rho^B)^2 + \frac{\zeta}{2}((\rho^A)^2 - (\rho^B)^2) + \omega(\rho^A+\rho^B)^3\right\}\mathrm{d}\vec{r} \quad (2)$$

in the segment number densities. It contains the following parameters: ν = excluded volume, χ = incompatibility, ζ = solvent selectivity. The last two parameters are dimensionless. We also include a single third virial parameter, ω. The parameter χ is proportional to the Flory−Huggins parameter, and it describes the incompatibility of the two polymers. Positive values of the solvent selectivity parameter ζ indicate that the solvent is better for *A* chains than for *B* chains.

The free energy functional (1) is minimized with respect to the segment densities ρ^A, ρ^B and the effective fields w^A, w^B. We solve the problem in Fourier space: densities and fields are expanded in a Fourier series of basis functions with the symmetry of the phase under consideration. We calculate the properties of the system in a patch of lateral size *L* and height $2.3h_\theta{}^A$. In the case of a laterally structured morphology this patch comprises one unit cell of the lateral structure. Therefore, unlike the experiment, we only consider perfectly periodic lateral structures. For each calculation we minimize the free energy with respect to the lateral size *L* of the unit cell. Because of the limited number of 200 basis functions in the Fourier expansion, we cannot describe very sharp interfaces. The self-consistent equations for the expansion coefficients are solved via a Newton−Broyden algorithm. Further details of the calculations can be found elsewhere.[31] In our study we consider the cases of a neutral solvent, $\zeta = 0$, and a solvent, selective for the *B* component, $\zeta = -0.2$. The grafting density σ, the excluded volume ν, and the number of segments *N* per chain enter into the calculations only in the combination $\delta^{-3} = {}^3/_2(\nu N^2/h_\theta{}^{A\,3})^2(\sigma h_\theta{}^{A\,2})^2$. For our calculations we use the value $\delta = 0.46$, which corresponds to intermediate stretching (cf. Figure 1 for a density profile of the components) and $\omega = 0.1\nu N\delta$.

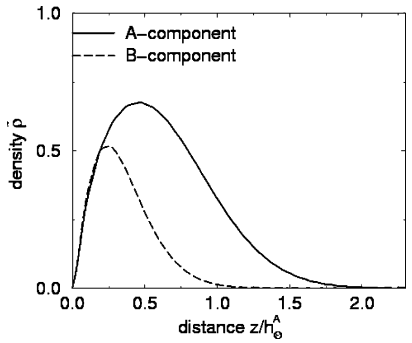

Figure 1. Density profiles of the *A* component (solid line) and *B* component (dashed line) of the reference brush. *A* and *B* chains are chemically identical (reference case, $\zeta = 0$, $\chi = 0$) but differ in size, $\alpha = 0.4$. The density is shown in scaled units $2h_\theta{}^A/(N\sigma)({}^2/_3\delta)^{1/2}$.

We caution the reader that our simplistic virial ansatz for the equation of state is only a crude representation of mixtures of two polymers and a selective solvent. Moreover, the finite number of Fourier terms limits our calculations to weak and intermediate segregation. In the experiment one observes the frozen morphology after drying. During the rapid evaporation of the solvent, the polymer density (and therefore also the incompatibility parameter χ in our model) increases, and the brush morphology arrests in a glassy state. This frozen state contains information about the equilibrium structure at some (unfortunately, not very well-known) solvent concentration. Thus, even if the true equation of state for the mixture of two incompatible polymers in a common solvent was known, there would still be an uncertainty in the solvent concentration to be used in the comparison with experiments. At any rate the experiments presumably correspond to a fairly large incompatibility. For these reasons we can aim at a *qualitative* comparison between SCF calculations and experiments only.

In this paper we restrict ourselves to the hexagonal symmetry (dimple phase), which is most likely to minimize the free energy for the parameters investigated. We have verified for selected parameters that the ripple phase has a larger free energy. In the latter, the components segregate into cylinders that run parallel to the grafting surface.[30a] This observation is in accord with the observation of rather spherical clusters (as opposed to elongated ones) without long-range order in previous experiments with PS/P2VP brushes in a selective solvent.[32] In the dimple morphology, one of the components forms clusters or passages arranged on a triangular lattice, and the other component forms a honeycomb matrix (Scheme 1). The chain size asymmetry is parametrized as a squared ratio of the chains' end-to-end distances in a θ-solvent, $\alpha = (h_\theta{}^B/h_\theta{}^A)^2$. In our SCF calculations the size of the *A* chains ($h_\theta{}^A$) is fixed and taken to be the unit of length. The size of the *B* chains ($h_\theta{}^B$) is varied.

First we consider the limit when *A* and *B* chains are of identical chemical structure but differ in their sizes, i.e., $\chi = \zeta = 0$. We consider this case as a reference.[13−20] Then we study mixtures that differ in both size and chemical architecture. The latter is parametrized by the incompatibility, and we use the value $\chi = 3.65$. This

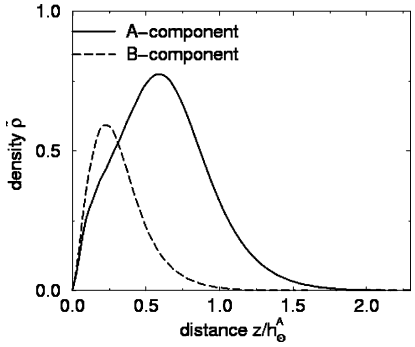

Figure 2. Density profiles for the brush consisting of chemically different chains ($\chi = 3.65$) of different sizes ($\alpha = 0.4$) in a selective solvent ($\zeta = -0.2$): *A* component (solid line) and *B* component (dashed line). The density is shown in scaled units $2h_\theta^A/(N\sigma)(^2/_3\delta)^{1/2}$.

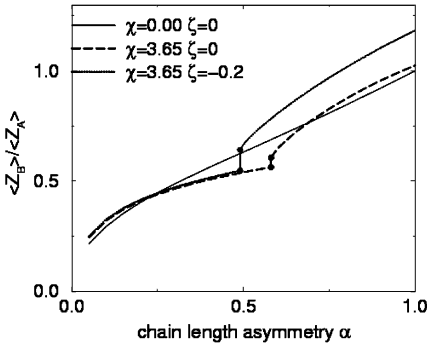

Figure 3. Ratio of the average distances of the *A*, *B* chains from the grafting plane via the chain size asymmetry, α: *A*, *B* are chemically identical (the reference system) (thin solid line); *A*, *B* are chemically different ($\chi = 3.65$), and the solvent is neutral ($\zeta = 0$) (thick solid line); the chemically different chains in a selective solvent ($\zeta = -0.2$) (thick dashed line). First-order transitions are marked by circles.

results in a hexagonal dimple morphology for binary brushes of equal chain sizes.[31]

Our SCF calculations explore the role of incompatibility and solvent selectivity on the structure and surface properties and compare the behavior to the reference case of chemically identical chains. First, comparing the laterally averaged density profiles of the compatible reference brush (Figure 1) and the incompatible brush (Figure 2), we observed that the mutual repulsion between the different components strongly influences the shape of the profiles and the position of the maximum density.

The longer *A* chains are pushed away from the grafting surface and dominate the top of the brush, while the shorter *B* chains predominantly occupied the bottom of the brush and do not reach the top. As the chain length asymmetry decreases, the profiles of the two components become more similar; i.e., the position of maximal density for the shorter chains moves outward. In Figure 3 we plot the ratio of the average distance of the *B* and *A* components from the grafting plane, $\langle Z_B\rangle/\langle Z_A\rangle$, as the function of the asymmetry parameter α. For the reference brush (thin solid line) the density profile of the *B* component gradually approaches that of the *A* component as α tends to unity. For incompatible components the ratio exhibits a discontinuity which corresponds to the first-order transition from a laterally homogeneous, layered state (sandwich structure, cf. Figure 4, top) for small values of the asymmetry parameter α to a laterally structured morphology (cf. Figure 4, bottom).

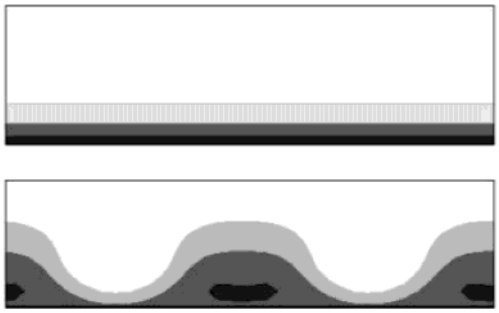

Figure 4. Contour plot (side view) of the fraction of the *B* segment relative density, $\tilde{\rho}^B = \tilde{\rho}^B/(\rho^A + \rho^B)$, below (top) and above (bottom) the phase transition from the laterally homogeneous to the laterally structured phases at $\alpha \cong 0.49$ in a selective solvent, $\zeta = -0.2$. Gradations of gray from light to dark correspond to the increasing of the relative density of the *B* component.

These contour plots explain the reason for the different dependence of the ratio $\langle Z_B\rangle/\langle Z_A\rangle$ on α below and above the phase transition point: as the lateral homogeneity is broken, the *A* chains do not pass through the mixed region close to the grafting surface laterally homogeneously, but rather form passages that arrange on a triangular lattice. These passages are embedded into a *B*-rich matrix. In this morphology the *B* component more easily reaches the top of the brush. Therefore, we observe a stepwise increase of the ratio $\langle Z_B\rangle/\langle Z_A\rangle$ at the transition from the laterally homogeneous structure to the hexagonal structure. Upon increasing the chain length asymmetry α further toward unity, the fraction of *A* on the top of the brush decreases, and the *A*-rich passages gradually transform to clusters that are located close to the grafting surface.

The position of the transition between the laterally homogeneous and ordered state depends on the solvent selectivity. A solvent selective for the *B* component pushes the *B* chains outward, and the *A* chains are pulled closer toward the grafting surface. This increases the mixing of the shorter *B* chains and the longer *A* chains. As a consequence, the brush undergoes the phase transition at smaller values of α as compared to a neutral solvent. The inverse holds true when the solvent is selective for the *A* component (data not shown): in this case the solvent favors a stronger segregation of the brush components perpendicular to the grafting surface (sandwich structure), and the chain lengths have to be more similar to result in a sufficient degree of mixing (in the laterally homogeneous state) and to cause lateral microphase separation.

The surface properties of the brush, for example wettability or adhesion, depend mainly on the chemical composition of the brush's top layer. The extension of the top layer depends on the specific experimental probe. In our study we define that the top layer consists of 33% of the total amount of the *A* and *B* segments. To keep this value constant, the thickness of the top layer was adjusted for every set of the parameters. This identification is somewhat arbitrary, but we do not expect the specific definition to change our qualitative observations. The fraction of *B* segments in the top layer is shown in Figure 5a as a function of α. Above the phase transition the concentration of *B* segments in the top layer increases faster. Note that even for $\alpha = 1$ (i.e., equal chains) and a neutral solvent, $\zeta = 0$, the composi-

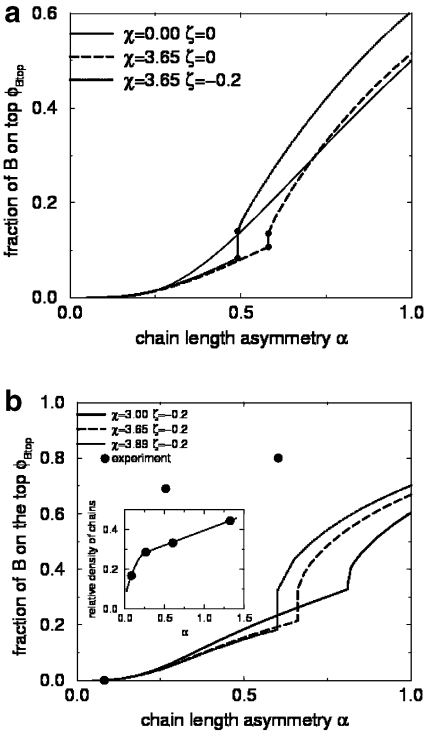

Figure 5. (a) Fraction of the *B* segments in the top layer of the brush (see our definition of the top layer in the text): *A*, *B* are chemically identical (the reference system) (thin solid line); *A*, *B* are chemically different ($\chi = 3.65$), and the solvent is neutral ($\zeta = 0$) (thick solid line); chemically different chains in a selective solvent ($\zeta = -0.2$) (thick dashed line). First-order transitions are marked by circles. (b) Fraction of the *B* segments in the top layer of the brush. Comparison of the experimental data (filled points) and the SCF calculations. The fraction of grafted *A* chains depends in the experiment on the chain length asymmetry (inset). This dependence is employed in the SCFT calculations in order to compare with the experiment.

tion of the top layer does not equal 0.5. In the "dimple *A*" morphology the matrix-forming component *B* is enriched at the top.

Structure and phase behavior of a mixed brush depend on the composition of the brush. To isolate the interplay between solvent selectivity and chain length asymmetry, we have restricted ourselves to symmetric composition. In the experiment, however, the grafting density of PS is larger than that of P2VP, and it varies upon changing the chain length asymmetry (cf. Table 2). To mimic the experimental situation, we account for the experimental dependence of the density fraction of the *A* component on the chain length asymmetry (cf. inset of Figure 5b) in our SCF calculations. Figure 5b demonstrates that the dependence of the fraction of the *B* component in the top layer of the brush is *qualitatively* the same as for the case of the symmetric grafting density (cf. Figure 5a). The phase transition to the laterally ordered phase occcurs at higher values of the chain length asymmetry α compared to the case of symmetric grafting density. The possible explanation is the lower degree of mixing of the polymers of two types, when one of them is in the majority. The figure illustrates also that the position of the first-order transition depends strongly on the degree of incompatibility of the polymers. For larger values of incompatibility χ, the transition occurs at smaller values of α, and the discontinuity of the surface composition is larger. We plan to explore the effect of the grafting density asymmetry in more detail in our future work.

Synthesis of Brushes. We synthesize our samples according to the three-step procedure detailed in the Experimental Section. First, we covalently grafted GPS to the surface of Si wafers. Second, we prepared five different mixed brushes by grafting PS of five different molecular weights. In the third step we grafted P2VP of the same molecular weight on each Si wafer with previously grafted PS. Each step of grafting was monitored with ellipsometry. The compositions of the mixed brushes are compiled in Table 1.

In addition to the absolute values presented in Table 1, and the parameter α introduced in the SCF section, we introduce two additional ratios to characterize the synthesized brushes: $R_\Sigma = \Sigma^{P2VP}/\Sigma^{PS}$ reflects the molecular composition or the grafting density asymmetry of the brushes, and $R_h = [(1/\Sigma^{PS} + 1/\Sigma^{P2VP})^{0.5}]/[(h_\theta{}^{PS} + h_\theta{}^{P2VP})/2]$ characterizes stretching of polymer chains in the brushes. The smaller R_h, the stronger the chains are stretched in the brush. We study here the effect of chain length asymmetry α on the brush properties. However, only one of the two other ratios can be kept constant in the experiment. We selected the samples such that they are characterized by approximately constant values of R_h because stretching of chains affects strongly the segmental density profiles and thereby the incompatibility. It was demonstrated elsewhere[33,34] that if both polymers in the mixed brush have the same molecular mass, the brush composition within the range of R_Σ from 0.2 to 4 has a comparably small effect on the switching behavior in selective solvents. In this paper we use a much smaller variation of R_Σ ranging from 0.2 to 0.7. Thus, all investigated brushes have similar values of R_h, differ slightly in R_Σ, but are distinguished by large variation in the chain length asymmetry α.

Switching properties of the brushes were studied by exposing the samples to selective solvents for one of polymers (toluene for PS and ethanol for P2VP) for 10 min. Then samples were dried rapidly under nitrogen flux as described elsewhere.[33,34] The brush structure, frozen into a glassy state by rapid solvent evaporation, was investigated using water contact angle measurements (CA) and SPM. The results of contact angle measurements are shown in Table 2.

For α in the range from 0.27 to 2.05 we find no substantial effect of the brush composition and chain length asymmetry on the switching between different surface compositions after exposure to toluene or ethanol. The composition of the brush's top can be inferred by comparing the contact angle of water drops on the brush to its value for pure polymer films, 90° for PS and 60° for P2VP. In ethanol the top layer is enriched with P2VP. For most samples P2VP has also the larger molecular weight, and this result is expected as chain length asymmetry and solvent selectivity both favor P2VP at the top. However, we also observe an enrichment for $\alpha = 2.05$, i.e., in the case that the PS chains are longer than P2VP. From the contact angle we estimate the P2VP fraction on the top to be 0.85. In toluene—selective solvent for PS—PS is enriched on the top of the brushes (cf. Table 2). Note that solvent selectivity and chain length asymmetry oppose each other for $\alpha < 1$, but the solvent selectivity dominates the behavior up to $\alpha = 0.27$.

Table 1. Composition and Structure of the PS/P2VP Mixed Brush

M_W, g/mol		h_θ, nm			A, mg/m^2		Σ, nm^{-2}				intercluster distance L, nm	
PS	P2VP	PS	P2VP	α	PS	P2VP	PS	P2VP	R_Σ	R_h	predicted	experiment
2 980	41 500	3.8	13.4	0.08	1.2	3.4	0.24	0.049	0.2	0.14	18	
9 700	41 500	6.9	13.4	0.27	1.8	2.9	0.11	0.042	0.4	0.25	21	41
21 900	41 500	10.4	13.4	0.60	3.7	3.7	0.10	0.053	0.5	0.21	25	35
48 700	41 500	15.4	13.4	1.32	3.8	2.7	0.047	0.039	0.8	0.24	30	48
75 200	41 500	19.2	13.4	2.05	5.6	2.1	0.045	0.03	0.7	0.22	35	65

Table 2. Switching of Surface Energetic State of the Brushes

M_W				water contact angle, deg		fraction of P2VP on the surface		fraction of PS on the surface	
PS	P2VP	α	R_Σ	after toluene	after ethanol	after toluene	after ethanol	after toluene	after ethanol
2 980	41 500	0.08	0.2	60	[60]	1	1	0	0
9 700	41 500	0.27	0.4	81	63	0.31	0.91	0.69	0.09
21 900	41 500	0.60	0.5	84	65	0.20	0.85	0.80	0.15
48 700	41 500	1.32	0.8	85	64	0.17	0.88	0.83	0.12
75 200	41 500	2.05	0.7	90	65	0	0.85	1	0.15

For α = 0.08 (the first line in Table 2) we observed no switching, and the surface was always hydrophilic even after exposure to toluene. This suggests that the effect of solvent selectivity is not enough to overcome the tendency of the longer species to enrich at the top.

These results are in qualitative agreement with the findings of the SCF calculations: A decrease of the molecular mass asymmetry stabilizes the ability of the brush to switch its surface composition. If the chain length asymmetry is, however, very large, the brush adopts a sandwich-like structure (strong perpendicular segregation but laterally homogeneous) where the longer chains are enriched on the top.

Morphology of the brushes was studied with SPM in the tapping mode applying two different regimes: light and moderate tapping.[35,36,38] The comparison of images recorded in the different modes (in junction with the contact angle measurements) helps to infer information about perpendicular and lateral segregation in the brushes.

The light tapping regime is realized when the scanning is conducted at the highest set-point value that permits a reproducible imaging. During the light scanning mode, the tip−sample interaction is strongly influenced by attractive adhesion forces. The regime allows for nondestructive probing of the very top layer of the brush. Moderate tapping is carried out at lower set points, and thus higher forces are applied to the sample. Therefore, in this case, topography images frequently do not reflect the actual surface morphology because the rigid silicon tip exerts high forces to the polymer film that might squeeze the topmost layer and might create additional (spurious) surface corrugations. Figure 6 shows high-resolution topography images of the PS9K/P2VP45K brush after toluene treatment obtained in the light and moderate tapping modes. There are notable differences between the two images. In fact, some additional morphological features are created by the scanning with higher forces. Therefore, only phase images obtained in moderate tapping mode were analyzed in the present paper.

Once the AFM tip penetrates through the soft topmost layer during the moderate tapping, the tip interacts with the polymer segments situated somewhat deeper inside the brush. Then, the phase image that reflects tip/sample interactions contains some information about the film structure underneath the top surface. For the scanning with lower set point, the elastic forces due to the deformation of the sample can be described by an additive term to the spring constant of the cantilever−sample system.[39] As a consequence of the higher effective spring constant, the resonance frequency increases, which keeps the drive frequency constant, and the phase shift increases. For a soft sample the phase shift is smaller than for a stiff sample. Accordingly, a region of

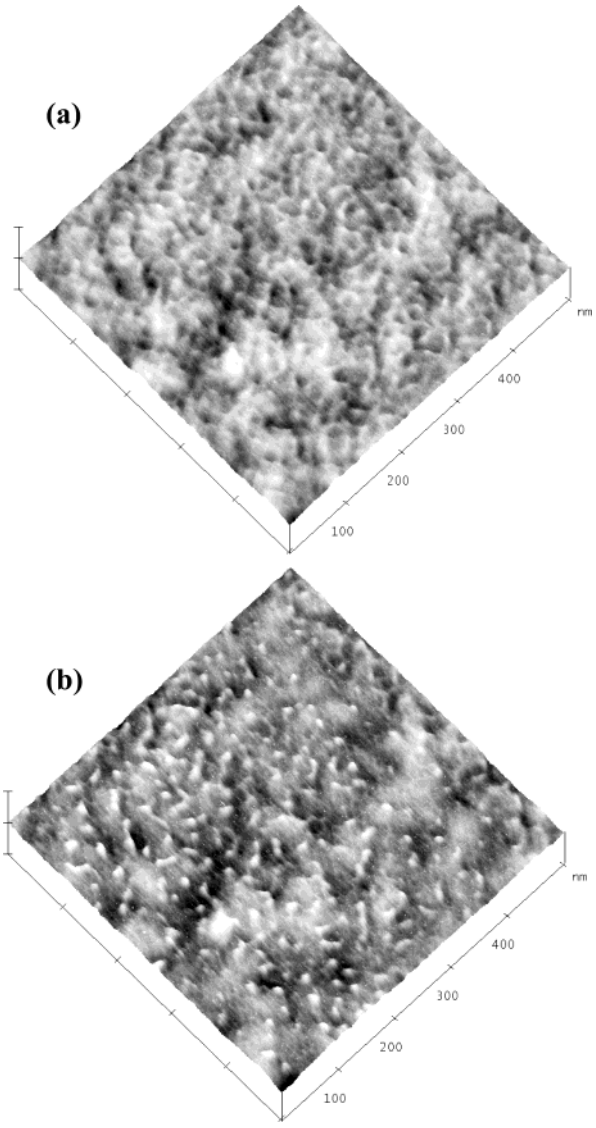

Figure 6. AFM topography images (500 × 500 nm) of PS9K/PVP45K brush after toluene treatment obtained in the light (a) and moderate tapping (b) modes. Vertical scale 10 nm.

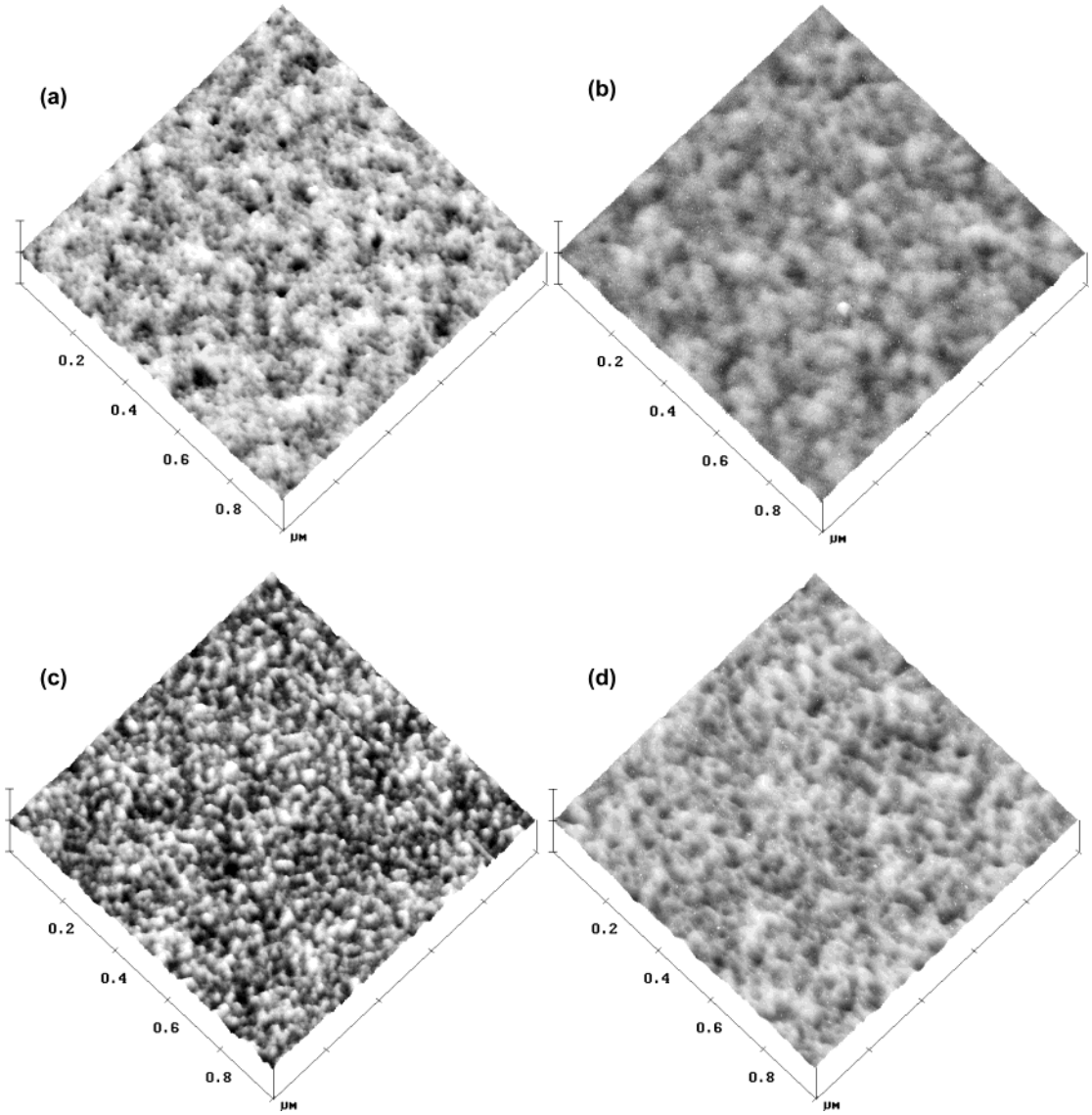

Figure 7. Dependence of surface morphology of the mixed brushes on molecular weight of grafted PS after treatment with THF. (a) PS2K, (b) PS9K, (c) PS45K, and (d) PS72K. Roughness: (a) 0.35, (b) 0.3, (c) 0.37, and (d) 0.3 nm. 1 × 1 μm AFM images; light tapping; vertical scale 10 nm.

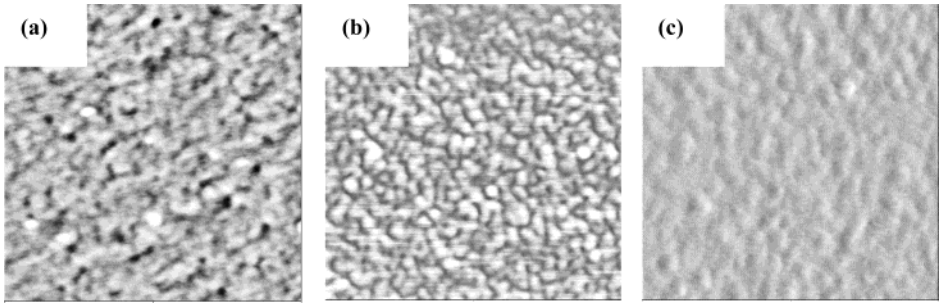

Figure 8. Phase images of the mixed brushes (500 × 500 nm) consisting of (a) PS2K, (b) PS9K, and (c) PS45K. The brushes were treated with toluene. Light tapping mode. Vertical scale 30°.

higher density appears brighter in the phase images recorded in the moderate scanning mode.

Topographical SPM images (light tapping) of the PS/P2VP mixed brushes after treatment with THF (*non-selective solvent*) are presented in Figure 7. The images reflect the initial morphology of the grafted layers obtained after grafting and treatment with THF in a Soxhlet apparatus. All brushes uniformly cover the substrate and possess a very fine surface texture. Only for the symmetric brush (PS45K/P2VP42K) formation of clusters on the brush surface is observed. The roughness (reported in the caption of Figure 7) is practically identical for all grafted layers studied.

Figure 8 displays *phase images* of mixed brushes treated with toluene (selective solvent for PS). The images were recorded in the light tapping mode. The contact angle measurements suggested that only P2VP segments were present on the surface of the PS2K/

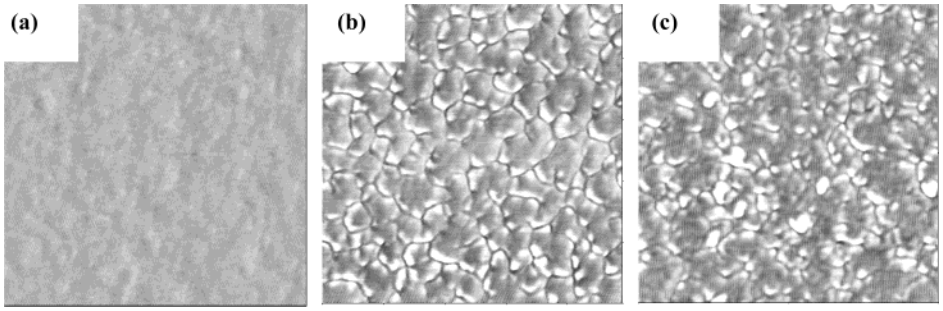

Figure 9. Phase images of the mixed brushes (500 × 500 nm) consisting of (a) PS2K, (b) PS45K, and (c) PS75K. The brushes were treated with ethanol. Light tapping mode. Vertical scale 30°.

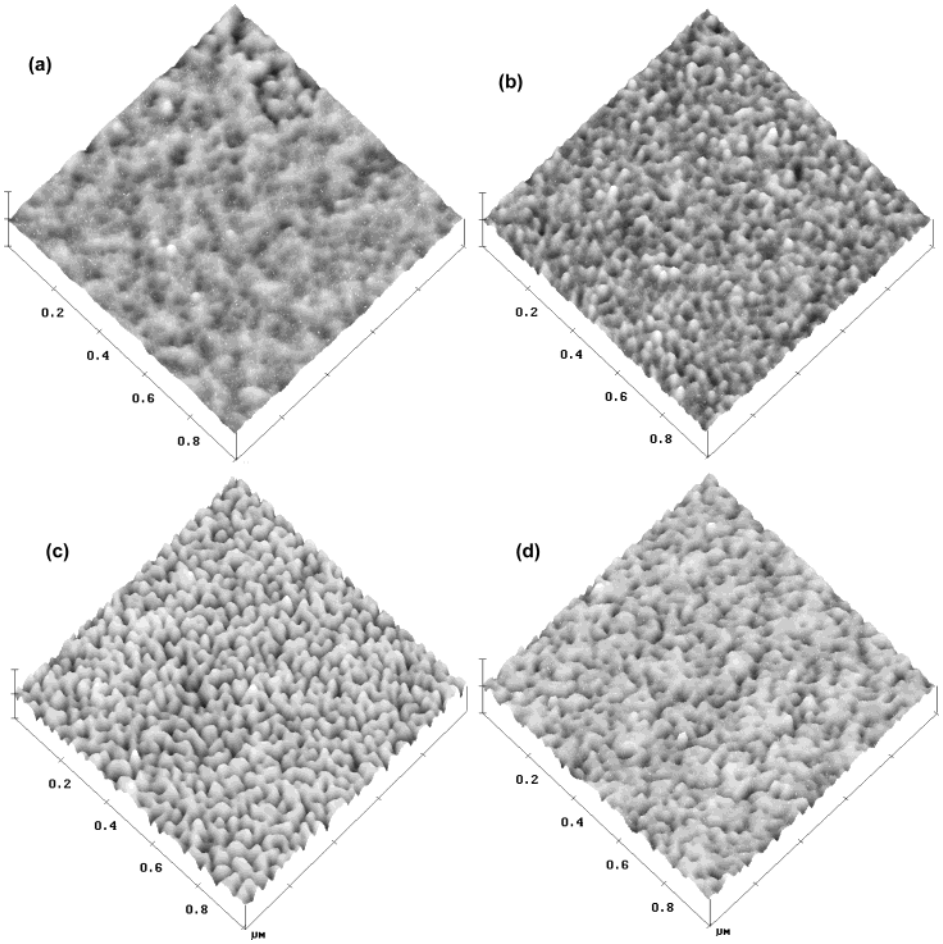

Figure 10. Dependence of surface morphology of the mixed brushes on molecular weight of grafted PS after treatment with ethanol. (a) PS2K, (b) PS9K, (c) PS45K, and (d) PS72K. Roughness: (a) 0.4, (b) 0.5, (c) 1, and (d) 0.7 nm. 1 × 1 μm AFM images; light tapping; vertical scale 10 nm.

P2VP42K brush (Table 2). However, the AFM phase image showed that a limited number of PS segments, which did not influence the contact angle measurements, was located on the brush top (Figure 8a). According to the contact angle measurements on the PS9K/P2VP42K brush, both PS and P2VP units were present on the top of the brush treated with toluene. In fact, we can detect surface regions with different adhesive interaction with AFM tip (Figure 8b). A virtually even distribution of adhesive forces on the brush surface was found for the grafted layer consisting of PS45K and PS75K (Figure 8c). This indicates that mostly PS segments were present at the brush surface. This observation correlates well with the contact angle data (Table 2). Figure 9 shows the AFM *phase images* for the mixed brushes treated with ethanol (selective solvent for P2VP) and recorded in the light tapping mode. For all samples but PS2K/P2VP42K evidence for a limited amount of PS segments was found on the brush top, in accord with the contact angle measurements (cf. Table 2).

Figures 10 and 11 show how the *surface morphology* of the mixed brushes changes with molecular weight of PS and solvent selectivity. The images were recorded in the light tapping mode. In this case the image reflects the morphology of the topmost layer. We observe that there is not much dependence of the surface structure on the solvent for the mixed brush containing the shortest PS chains. This observation corroborates our theoretical considerations and contact angle measurements. The samples consisting of longer PS molecules exhibit a significant variation of the surface structure

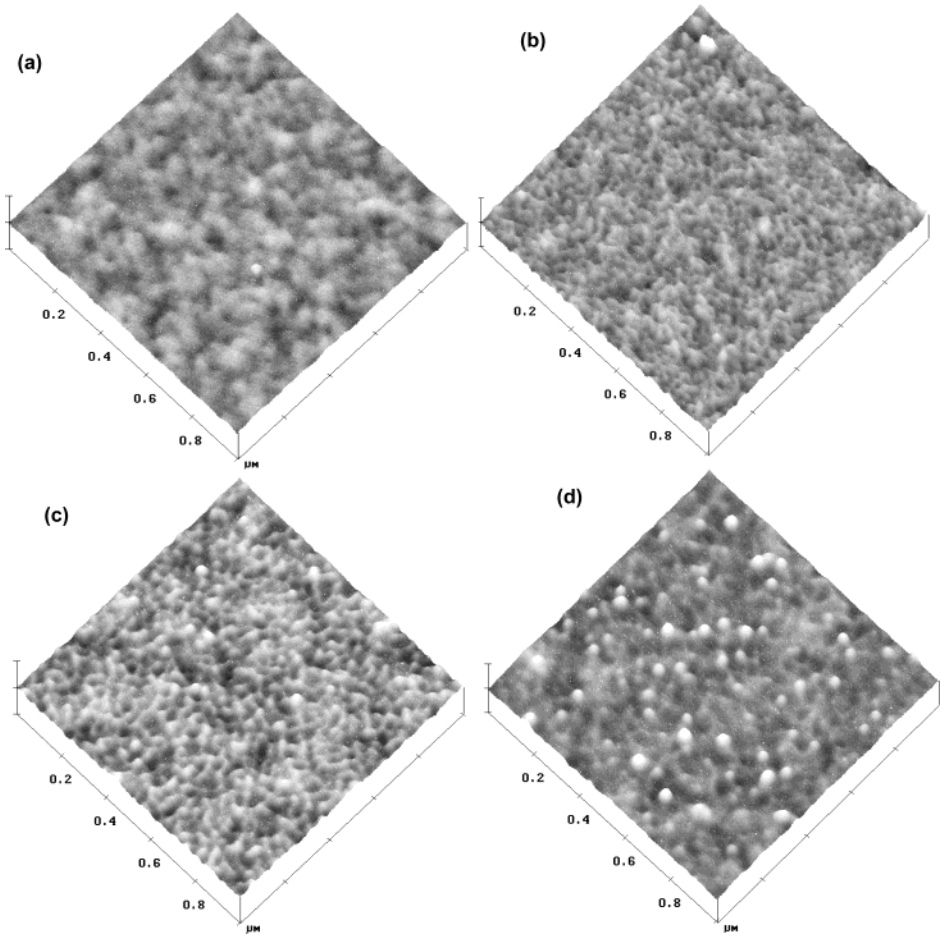

Figure 11. Dependence of surface morphology of the mixed brushes on molecular weight of grafted PS after treatment with toluene. (a) PS2K, (b) PS9K, (c) PS45K, and (d) PS72K. Roughness: (a) 0.4, (b) 0.4, (c) 0.4, and (d) 0.7 nm. 1 × 1 μm AFM images; light tapping; vertical scale 10 nm.

when the mixed brushes were exposed to various solvents. From a simple visual inspection it appears that when the polymers (PS and P2VP) constituting the brush have comparable molecular mass, the variation of the morphology is more pronounced.

Figures 12 and 13 present phase images of the mixed brushes exposed to toluene and ethanol, respectively. The images were recorded in the moderate tapping mode, as controlled by the dependence of the amplitude and phase shift on the distance between the sample and cantilever. This type of tapping at higher forces yields some information about the structure below the top layer. Indeed, we obtain evidence for lateral phase separation for all samples treated with toluene and ethanol. Comparing both SPM regimes and contact angle data, we may estimate the amount of lateral and perpendicular segregation.

The symmetric brush PS45K/P2VP42K exposed to toluene (Figures 11c and 13c) and ethanol (Figure 10c and 12c) exhibits in both cases—light (topography) and moderate tapping (phase) modes—clusters that are presumably formed by the species that are not preferred by the solvent. In addition to lateral segregation, perpendicular segregation occurs when the very top of the brush is enriched by the polymer that is favored by the solvent (Table 2, Figures 8 and 9). This perpendicular segregation results in the switching from hydrophilic (contact angle 64°) to hydrophobic states (contact angle 85°).

The asymmetric brush PS72K/P2VP42K (Figures 10d, 11d, 12d, and 13d) exhibits a different morphology. Effects of asymmetry are clearly visible if we compare the phase images taken after exposure to toluene and ethanol. Toluene (selective solvent for PS) enhances the perpendicular segregation, the top of the brush appears smooth at light tapping (Figure 11d), and it is composed mainly of PS (Table 2). However, moderate tapping (Figure 13d) additionally gives evidence for lateral segregation (dimple morphology). Upon exposure to ethanol (selective for P2VP) a different lateral morphology (ripple) is observed in light and moderate tapping mode images (Figures 10d and 12d). Similar results are obtained for the brush with inverse asymmetry PS9K/P2VP45K (Figures 10b, 11b, 12b, and 13b). There is, however, one difference: In the latter case a dimple morphology is observed after ethanol (Figure 12b), while a ripple morphology is observed after toluene (Figure 13b), in contrast to the brush PS72K/P2VP42K of inverse asymmetry.

The extremely asymmetric brush, PS2K/P2VP42K (Figures 10a and 11a), shows an almost smooth surface upon exposure to both toluene and ethanol. This indicates that perpendicular segregation dominates and lateral segregation is suppressed. The moderate tapping phase image (Figure 12a) shows that no lateral phase separation is observed under ethanol: The solvent and the chain length asymmetry favor perpendicular segregation. However, some limited degree of the lateral

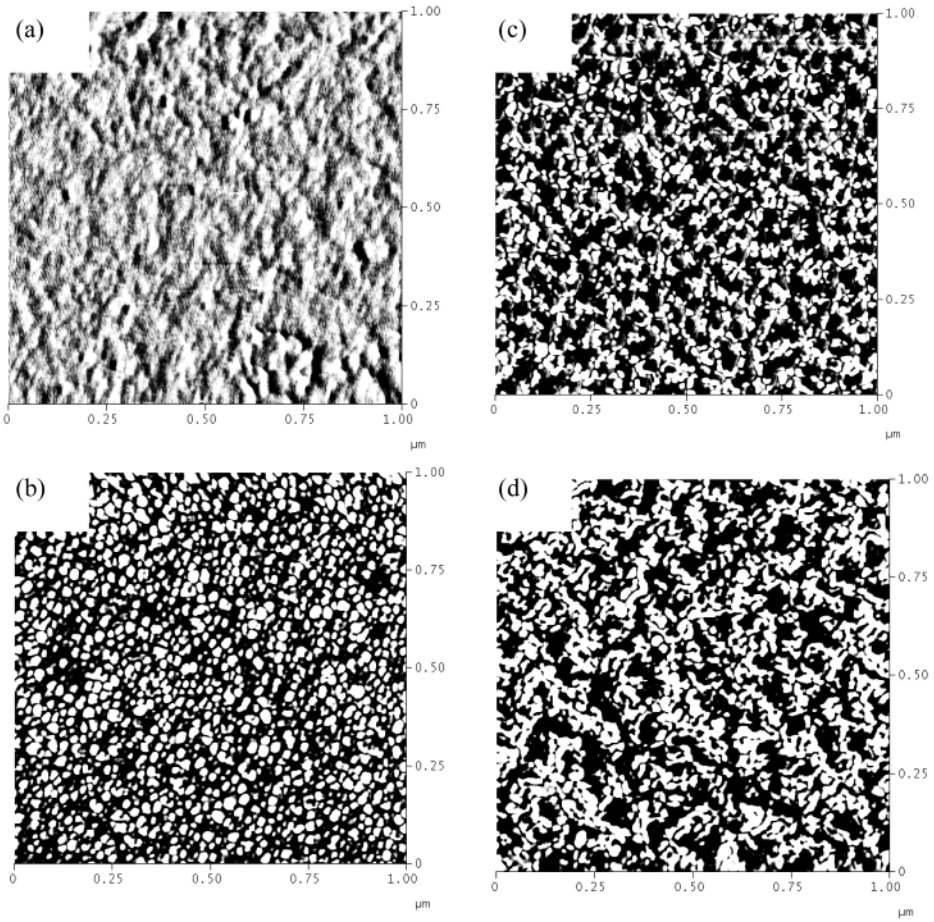

Figure 12. Phase images (1 × 1 μm) of the mixed brushes treated with ethanol: (a) PS2.98K, (b) PS9.7K, (c) PS48.7K, and (d) PS75.2K. Moderate tapping; vertical scale 10°.

structure is observed at moderate tapping, when the brush is treated with toluene (Figure 13a). In this case, the solvent selectivity opposes the chain length asymmetry in its tendency toward perpendicular segregation.

As mentioned above, when we vary the brush's molecular mass asymmetry, we simultaneously alter the brush's composition, keeping the grafting density roughly constant. Hence, both changes of α and R_Σ may change the morphology, enhance perpendicular segregation, or change the mechanism of lateral segregation. Above, we have mainly discussed an interplay between lateral and perpendicular segregation in response to changing the ratio of chain lengths α. However, from the SPM images we can also study the effect of the ratio of grafted chains R_Σ. Comparison of Figure 12b−d and Figure 13b−d reveals that they are inverse with respect to the relationship between layer composition, incompatibility, and morphology of segregated phases. Symmetric brushes in both solvents form ripple morphologies (Figures 12c and 13c). In asymmetric brushes, one component tends to form clusters embedded in the matrix of the other component (dimple morphology). This morphology is stabilized by solvent selective for matrix component. Thus, the PS75K/P2VP42K brush undergoes transition from ripple to dimple morphology in toluene (selective for longer PS chains), while the PS9K/P2VP42K brush undergoes the same transition in ethanol (selective for longer P2VP chains).

Comparing SCF Calculations and Experiment. Using experiments and SCF calculations, we have explored the dependence of the mixed brush's behavior on the size asymmetry of its components. Two different regimes for the density distribution and the chemical composition of the top layer of the brush on the size asymmetry parameter have been observed. For strong asymmetry (small α, in terms of our model) the brush adopts a layered structure (Scheme 2a) with the components well segregated perpendicular to the substrate. For smaller asymmetry (relatively large α), perpendicular and lateral microphase segregation (Scheme 2b) occur simultaneously. The two regimes are separated by the transition between the laterally homogeneous (disordered) and the laterally structured morphologies. Increase of the solvent selectivity increases the enhancement of the concentration of the short chain in the surface layer of the brush (Scheme 2c). The comparison of SCF calculations for a brush of compatible polymer species and incompatible ones shows that a sharp change of the brush properties upon varying the chain length asymmetry parameter is the characteristic behavior of the brush composed of *chemically different* short and long components.

For the parameters employed in the SCF calculations, the transition between the two states of the brush takes place at the chain length asymmetry $0.4 \leq \alpha \leq 0.6$. In the experiment with the PS/P2VP brush in toluene the transition to the layered regime with a PS-enriched surface occurs around $0.08 \leq \alpha \leq 0.26$ (Table 2). This quantitative discrepancy is not surprising in view of the difference between the SCF model and the experimental realization. Most notably, we did not incorporate any specific equation-of-state data into our SCF model, but

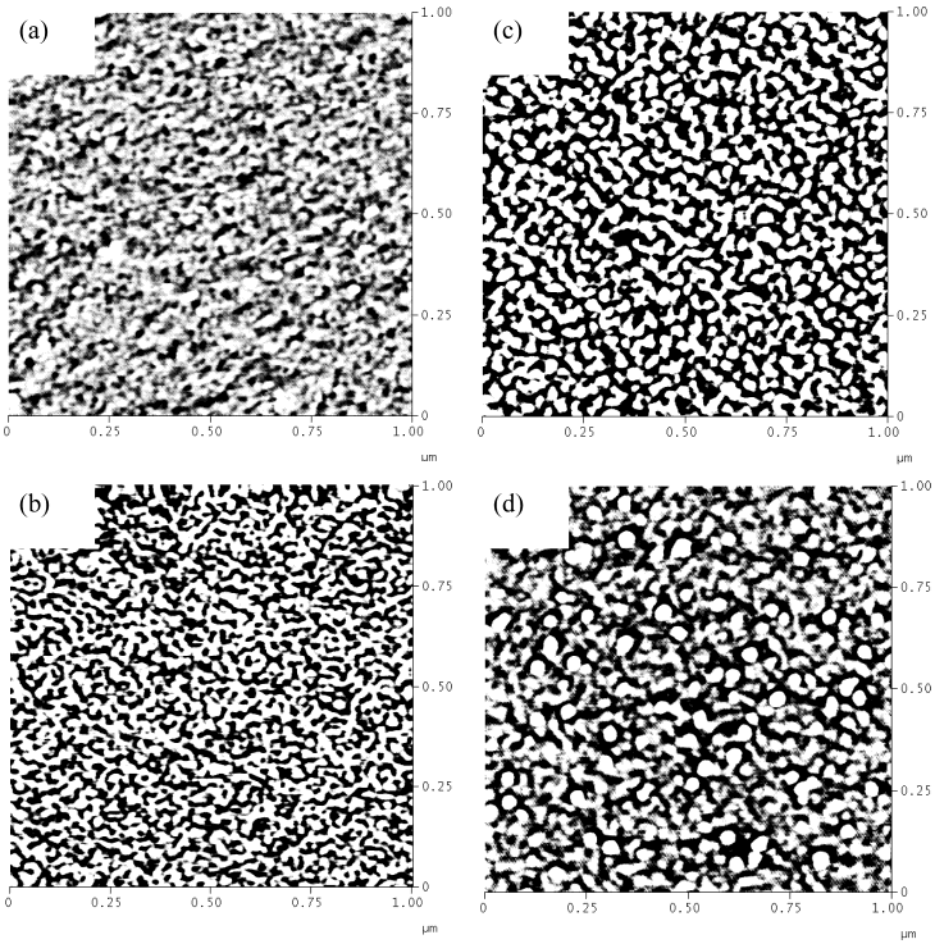

Figure 13. Phase images (1 × 1 μm) of the mixed brushes treated with toluene: (a) PS2.98K, (b) PS9.7K, (c) PS48.7K, and (d) PS75.2K. Moderate tapping; vertical scale 10°.

Scheme 2. Schematic Illustration of the Bidisperse Mixed Brush in Solvent Selective for Short Black Chains: Stratification Due to the Molecular Weight Asymmetry Acts against Solvent Selectivity and the Top Layer Is Occupied by Longer Chains (a), the Mixed Brush Undergoes Lateral Phase Segregation When Both Polymers Are on the Surface (b), and the Interaction with Solvent Dominates and Acts against the Stratification by Chain Length (c)

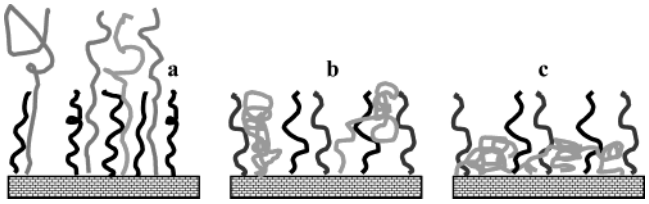

rather employed a generic third-order virial expansion. As we do not know the experimental equation of state for the specific mixture of PS/P2VP in toluene and ethanol, the parameters of the SCF model cannot be mapped quantitatively onto the experiment. Presumably, the incompatibility, solvent selectivity, and chain stretching are larger in the experiment than what we can consider in the numerical SCF scheme. Nevertheless, we expect the experimental system and the SCF calculations to share the same gross *qualitative* behavior.

Moreover, the change of the surface composition after the transition from the homogeneous structure to the laterally structured state is stronger in the experiment than in the SCF calculations. In addition to the reasons above, this effect additionally depends somewhat on the definition (extension) of the top layer. If we reduced the thickness of the top layer, the variation of the composition would become more pronounced in the SCF calculations.

To mimic the experimentally observed dependence of the relative grafting density of the components on the chain length asymmetry, we calculated the compositon of the brush's top varying grafting fraction of the *A* component and chain length asymmetry simultaneously (Figure 5b). This leaves the *qualitative* behavior unaltered. As we increase the incompatibility, the transitions occur at smaller α and are stronger first order, and the predictions of the SCF calculations tend in the direction of the experimental results.

We approximate the theoretically expected size of polymer clusters in the laterally segregated phases[31,32] via $L = k(h_{\theta PS}\,\varphi_{PS} + h_{\theta P2VP}\varphi_{P2VP})h_{\theta}^{A}$, where φ_{PS} and φ_{P2VP} are the molar fraction of PS and P2VP in the brush, respectively, and the factor *k* equals 2.2 and 1.9 for dimple and ripple phases, respectively. These values are compared with the experimental data extracted from the plots for SPM topographical images in Table 2. The experimental sizes are about 1.4 times larger than predicted. There are several possible reasons for this discrepancy. (i) The variation of the chain's extension with the solvent in the SCF model differs from the experiment. In bulk solution, chains will swell in a good solvent, an effect that is not captured in our SCF calculations. Moreover, the factor *k* increases with incompatibility. (ii) Fluctuations in the grafting densi-

ties and polydispersity might increase the lateral length scale. Recent Monte Carlo simulations suggest that fluctuations in the grafting density increase the size scale of the morphology.[40] (iii) To some extent, this difference can be traced back to inhomogeneity introduced by the "grafting to" method when phase segregation during the grafting procedure can introduce deviations from a random distribution of grafted points for both polymers. The strength of these spatial correlations in the experiment is unknown, and correlations cannot be incorporated easily in the SCF technique.

Conclusions

In view of the differences between the experimental system and the SCF model, we consider the qualitative agreement gratifying. Both approaches identify the same mechanism: the structure of the mixed polymer brush results from an interplay between solvent selectivity and chain length asymmetry. The solvent selectivity favors enrichment of the preferred component to the brush's top, and this tendency is opposed by the chain length asymmetry if the preferred species is smaller. If the chain length asymmetry is small, the solvent selectivity dominates and the brush responds to the solvent (switching). In this case the brush exhibits lateral and perpendicular segregation simultaneously. In the experiment this behavior is observed up to chain length ratios of order 4, while the maximal value of the asymmetry is smaller in the SCF calculations. For strong chain length asymmetry, the brush becomes laterally homogeneous, and the larger polymers are enriched at the top (sandwich structure).

Acknowledgment. Financial support was provided by the DFG: SFB 287, B 10. M.M. thanks the DFG for a Heisenberg stipend. This work was also supported in part by the Department of Commerce (USA) through the National Textile Center, M01-CL03 Grant, and the ERC Program of National Science Foundation under Award EEC-9731680.

References and Notes

(1) Halperin, A.; Tirrell, M.; Lodge, T. P. *Adv. Polym. Sci.* **1992**, *100*, 31−71 and references therein.
(2) Zhao, B.; Brittain, W. J. *Prog. Polym. Sci.* **2000**, *25*, 677−710 and references therein.
(3) Alexander, S. J. *J. Phys. (Paris)* **1977**, *38*, 983−987.
(4) de Gennes, P.-J. *J. Phys. (Paris)* **1976**, *37*, 1443. de Gennes, P.-J *Macromolecules* **1980**, *13*, 1069.
(5) Cantor, R. *Macromolecules* **1981**, *14*, 1186.
(6) Semenov, A. N. *Sov. Phys JETP* **1985**, *61*, 733.
(7) Milner, S. T.; Witten, T. A.; Cates, M. E. *Europhys. Lett.* **1988**, *5*, 413.
(8) Zhulina, E. B.; Borisov, O. V.; Pryamitsin, V. A. *Vysokomol. Soedin.* **1989**, *31A*, 185.
(9) Parsonage, E.; Tirrell, M.; Watanabe, H.; Nuzzo, R. *Macromolecules* **1987**, *20*, 1987.
(10) Cosgrove, T.; Heath, T. G.; Ryan, K.; Crowley, T. L. *Macromolecules* **1987**, *20*, 1361.
(11) Cosgrove, T.; Ryan, K. *Langmuir* **1990**, *6*, 1361.
(12) Auroy, P, Auvrey, L.; Léger, L. *Phys. Rev. Lett.* **1991**, *66*, 719.
(13) Milner, S. T.; Witten, T. A.; Cates, M. *Macromolecules* **1989**, *22*, 853.
(14) Birstein, T. M.; Liatskaya, Y. V.; Zhulina, E. B. *Polymer* **1990**, *31*, 2185.
(15) Chakrabarti, A.; Toral, R. *Macromolecules* **1990**, *23*, 2016.
(16) Dan, T.; Tirrell, M. *Macromolecules* **1993**, *26*, 6467.
(17) Lai, P.-Y.; Zhulina, E. B. *Macromolecules* **1992**, *25*, 5201.
(18) Spontak, R. J. *Macromolecules* **1994**, *27*, 6363.
(19) Skvortsov, A. M.; Klushin, L. I.; Gorbunov, A. A. *Macromolecules* **1997**, *30*, 1818.
(20) Borovinskii, A. L.; Khohlov, A. B. *Macromolecules* **1998**, *31*, 1180.
(21) Klein, J.; Kamiyama, Y.; Yoshizawa, H.; Israelachvili, J. N.; Fetters, L. J.; Pincus, P. *Macromolecules* **1992**, *25*, 2062.
(22) Kumacheva, E.; Kölein, J.; Pincus, P.; Fetters, L. J. *Macromolecules* **1993**, *26*, 6477.
(23) Dhoot, S.; Watanabe, H.; Tirrell, M. *Colloids Surf.* **1994**, *86*, 47.
(24) Dhoot, S.; Tirrell, M. *Macromolecules* **1995**, *28*, 3692.
(25) Gao.Z.; Ou-Yang, H. D. *ACS Symp. Ser.* **1993**, *532*, 70.
(26) Mayes, A. M.; Russell, T. P.; Deline, V. R.; Satija, S. K.; Majkrzak, C. F. *Macromolecules* **1994**, *27*, 7447.
(27) Kent, M. S.; Factor, B. J.; Satija, S.; Gallagher, P.; Smith, G. S. *Macromolecules* **1996**, *29*, 2843.
(28) Levicky, R.; Koneripylli, N.; Tirrell, M.; Satija, S. K. *Macromolecules* **1998**, *31*, 2616.
(29) Goedel, W. A.; Luap, C.; Oeser, R.; Lang, P.; Braun, C.; Steitz, R. *Macromolecules* **1999**, *32*, 7599.
(30) (a) Marko, J. F.; Witten, T. A. *Phys. Rev. Lett.* **1991**, *66*, 1541. (b) Lai, P.-Y.; Binder, K. *J. Chem. Phys.* **1992**, *97*, 586. (c) Lai, P.-Y. *J. Chem. Phys.* **1994**, *100*, 3351. (d) Brown, G.; Chakrabarti, A.; Marko, J. F. *Europhys. Lett.* **1994**, *25*, 239. (e) Soga, K. G.; Zuckermann, M. J.; Guo, H. *Macromolecules* **1996**, *29*, 1998. Zhulina, E.; Balazs, A. C. *Macromolecules* **1996**, *29*, 2667.
(31) Müller, M. *Phys. Rev. E* **2002**, *65*, 030802(R).
(32) Minko, S.; Müller, M.; Usov, D.; Scholl, A.; Froeck, C.; Stamm, M. *Phys. Rev. Lett.* **2002**, *88*, 035502-1.
(33) Sidorenko, A.; Minko, S.; Schenk-Meuser, K.; Duschner, H.; Stamm, M. *Langmuir* **1999**, *15*, 8349. Minko, S.; Usov, D.; Goreshnik, E.; Stamm, M. *Macromol. Rapid Commun.* **2001**, *22*, 206.
(34) Minko, S.; Patil, S.; Datsyuk, V.; Simon, F.; Eichhorn, K.-J.; Motornov, M.; Usov, D.; Tokarev, I.; Stamm, M. *Langmuir* **2002**, *18*, 289.
(35) (a) Luzinov, I.; Julthongpiput, D.; Malz, H.; Pionteck, J.; Tsukruk, V. V. *Macromolecules* **2000**, *33*, 1043. (b) Tsukruk, V. V.; Luzinov, I.; Julthongpiput, D. *Langmuir* **1999**, *15*, 3029. (c) Luzinov, I.; Julthongpiput, Liebmann-Vinson, A.; Cregger, T.; Foster, M. D.; Tsukruk, V. *Langmuir* **2000**, *16*, 504.
(36) Magonov, S. N.; Cleveland, J.; Elings, V.; Denley, D.; Whangbo, M.-H. *Surf. Sci.* **1997**, *389*, 201.
(37) Bar, G.; Thomann, Y.; Brandsch, R.; Cantow, H.-J.; Whangbo, M.-H. *Langmuir* **1997**, *13*, 3807.
(38) Pickering, J. P.; Vancso, G. J. *Polym. Bull. (Berlin)* **1998**, *40*, 549.
(39) Stapff, I.; Weidemann, G.; Shellenberg, C.; Rogenbreht, M.; Akari, S.; Antonietty, M. *Surf. Interface Anal.* **1999** *27*, 392. Spatz, J. P.; Sheiko, S.; Möler, M.; Winkler, R. G.; Reineker, P.; Marti, O. *Nanotechnology* **1995**, *6*, 40. Spatz, J. P.; Sheiko, S.; Möler, M.; Winkler, R. G.; Reineker, P.; Marti, O. *Langmuir* **1997**, *13*, 4699.
(40) Wenning, L., private communication.

MA034160H